

Structure, Stability, and Aggregation of Paired Helical Filaments from Tau Protein and FTDP-17 Mutants Probed by Tryptophan Scanning Mutagenesis*

Received for publication, June 25, 2002, and in revised form, August 16, 2002
Published, JBC Papers in Press, August 26, 2002, DOI 10.1074/jbc.M206334200

Li Li, Martin von Bergen, Eva-Maria Mandelkow, and Eckhard Mandelkow‡

From the Max-Planck-Unit for Structural Molecular Biology Notkestrasse 85, 22607 Hamburg, Germany

By using tryptophan scanning mutagenesis, we observed the kinetics and structure of the polymerization of tau into paired helical filaments (PHFs) independently of exogenous reporter dyes. The fluorescence exhibits pronounced blue shifts due to burial of the residue inside PHFs, depending on Trp position. The effect is greatest near the center of the repeat domain, showing that the packing is tightest near the β -structure inducing hexapeptide motifs. The tryptophan response allows measurement of PHF stability made by different tau isoforms and mutants. Unexpectedly, the stability of PHFs is quite low (denaturation half-points ~ 1.0 M GdnHCl), implying that incipient aggregation should be reversible and that the observed high stability of Alzheimer PHFs is due to other factors. The stability increases with the number of repeats and with tau mutants promoting β -structure, arguing for a gain of toxic function in frontotemporal dementias. Fluorescence resonance energy transfer (FRET) was used to analyze the distances of Tyr³¹⁰ to tryptophans in different positions. The degree of FRET in the soluble protein was position-dependent, with highest signals within the second and third repeats but low or no signals further away. In PHFs most mutants showed FRET, indicating that tight packing results from assembly of tau into PHFs.

Paired helical filaments (PHFs)¹ bundled into neurofibrillary tangles form one of the hallmarks of Alzheimer's disease and other neurodegenerative diseases. Their main constituent is the protein tau in a highly phosphorylated form. Tau normally functions as a microtubule-associated protein that is involved in microtubule stabilization and neurite outgrowth (1, 2). In principle, tau is one of the most soluble proteins of the brain, and therefore one of the key issues in molecular Alzheimer's research is the question of how and why tau becomes insoluble and aggregates into PHFs. To study this, one has to measure tau aggregation *in vitro*, and one has to develop assays to detect the aggregation rapidly and quantitatively. Such assays could then be used to study the factors that lead to tau aggregation,

and to search for reagents that inhibit aggregation and could therefore be used in prevention or therapy.

Human tau is coded by a single gene located on chromosome 17. Early in development there is only one isoform, the smallest "fetal" isoform htau23 (352 residues). During neuritogenesis, six main isoforms are generated in the human central nervous system by alternative splicing, the largest being htau40 (441 residues, Fig. 1) (3–5). One additional higher molecular form is generated in peripheral nerves (big tau). The six main isoforms in the central nervous system are distinguished by the presence or absence of two near-N-terminal inserts (coded by exons 2 and 3) and the second of four semi-conserved repeated motifs of 31–32 residues in the C-terminal half (coded by exon 10). One broadly distinguishes two major domains of tau, the C-terminal "assembly domain" and the N-terminal "projection domain." The assembly domain binds to microtubules through the 3 or 4 repeated motifs (R1–R4) and the adjacent proline-rich sequences; the projection domain is not involved in microtubule binding, points away from the microtubule surface, and may serve other functions that are presently not well understood. The repeat domain plays a dual role; it is not only involved in microtubule stabilization but also forms the core of Alzheimer PHFs after pathological aggregation (3, 6–8).

PHFs resembling those of Alzheimer's disease have been assembled from recombinant tau *in vitro*. This process is usually very slow (days or weeks), corresponding to the highly soluble nature of tau, and the verification of a *bona fide* PHF-like structure requires extensive structural characterization (electron microscopy, x-ray scattering, CD, or Fourier transformed infrared spectroscopy). Several principles have emerged over the past few years. The repeat domain is important for PHF aggregation (9–12); aggregation is strongly favored by oxidation that leads to tau dimerization by disulfide cross-links at Cys³²² (9, 13); aggregation is also strongly enhanced in the presence of polyanions such as heparin, ribonucleic acids, or acidic peptides such as poly(Glu) (12, 14, 15). Based on these principles, an assay of PHF aggregation *in vitro* has been developed that can be used in solution and in real time (16). It is based on the fact that the fluorophore thioflavine S added to the aggregation solution, strongly increases its fluorescence yield when PHFs are formed. This opened up the possibility of performing kinetic studies of PHF aggregation; for example, it was shown that the aggregation process follows a nucleation-elongation mechanism (17, 18). Although the ThS assay works reproducibly, it is conceptually not ideal because it relies on an exogenous reagent that could possibly alter some features of the aggregation pathway.

We have therefore searched for aggregation assays based on signals that are intrinsic to tau protein. In many cases, internal fluorophores provide signals when the fluorescence yield or excitation and emission spectra respond to the reaction proc-

* This project was supported in part by the Deutsche Forschungsgemeinschaft. The costs of publication of this article were defrayed in part by the payment of page charges. This article must therefore be hereby marked "advertisement" in accordance with 18 U.S.C. Section 1734 solely to indicate this fact.

‡ To whom correspondence should be addressed. Tel.: 49-40-89982810; Fax: 49-40-89716822; E-mail: mand@mpasmb.desy.de.

¹ The abbreviations used are: PHF, paired helical filament; FTIR, Fourier-transformed infrared spectroscopy; PBS, phosphate-buffered saline; ThS, thioflavine S; FRET, fluorescence resonance energy transfer; FTDP-17, Frontotemporal dementias and parkinsonism linked to chromosome 17; GdnHCl, guanidine hydrochloride.

ess. For proteins, such intrinsic signals are essentially restricted to tyrosine and tryptophan residues. Recently some studies (19, 20) showed similar approaches for other amyloids. Tau contains 5 Tyr residues but no Trp. We therefore explored the response of the Tyr fluorescence to the aggregation of tau into PHFs, and we show here that it can indeed be used to monitor the process. However, a much clearer signal is obtained from Trp. Because wild-type tau contains no Trp, it has to be introduced by site-directed mutagenesis. We used its fluorescence as a reporter to obtain new insights into the conformation of tau in the soluble state and after incorporation into PHFs. We show that the Trp fluorescence can be used to determine the stability of PHFs, their solvent accessibility (a measure of the compactness of PHFs), and the proximity of Trp and Tyr residues, as seen by fluorescence resonance energy transfer (FRET).

EXPERIMENTAL PROCEDURES

Chemicals and Proteins—Heparin (average M_n of 3000) and thioflavine S were obtained from Sigma. Human tau isoforms and constructs (see Fig. 1) were expressed in *Escherichia coli* as described (21). The numbering of the amino acids is that of the isoform htau40 containing 441 residues (22). The protein was expressed and purified as described by making use of the heat stability and fast protein liquid chromatography Mono S (Amersham Biosciences) (23). Separation of the monomeric and dimeric protein of htau39-Y310W was performed by applying protein samples in PBS on a Superose 12 PC 3.2/30 column (Amersham Biosciences) under control of the Smart-HPLC System (Amersham Biosciences) with a flow rate of 50 $\mu\text{l}/\text{min}$. The purity of the protein fractions was analyzed by SDS-PAGE. Protein concentrations were determined by the Bradford assay. The mutations of K18 (Q244W, L266W, Δ K280, Δ K280-Y310W, I297W, Y310W, I328W, and I360W), K19 (Y310W), htau40 (Y310W), and htau39 (Y310W) were created by site-directed mutagenesis, which was performed using the Quick Change kit (Stratagene, Germany) and the plasmid pNG2 (24). Plasmids were sequenced on both strands.

PHF Assembly—Aggregation was induced by incubating varying concentrations of tau isoforms or tau constructs (typically in the range of 50–100 μM) in volumes of 20–500 μl at 37 $^\circ\text{C}$ in PBS, pH 7.4, containing the anionic cofactor heparin. The ratio of heparin:protein was roughly 1:4 as described (17, 24). Incubation time varied between minutes up to several days. The formation of aggregates was ascertained by thioflavine S fluorescence and electron microscopy.

Thioflavine S Fluorescence Spectroscopy—Fluorescence was measured with a Fluoroskan Ascent (Labsystems, Germany) with an excitation filter of 440 nm and an emission filter of 510 nm in a 384-well plate. Measurements were carried out at room temperature in PBS, pH 7.4, and 10 μM ThS unless otherwise stated. Background fluorescence and light scattering of the sample without ThS was subtracted when needed.

Electron Microscopy—Protein solutions were diluted to 1–10 μM , and proteins were placed on 600-mesh carbon-coated copper grids for 1 min, washed with 2 drops of H_2O , and negatively stained with 2% uranyl acetate for 45 s. The specimens were examined in a Philips CM12 electron microscope at 100 kV.

Light Scattering—Microtubule assembly was monitored by light scattering at an angle of 90 $^\circ$ and 350 nm wavelength on a Kontron spectrophotometer (Kontron Instruments, Germany). 5 μM tau was mixed with 30 μM tubulin dimer at 4 $^\circ\text{C}$. The reaction was started by raising the temperature to 37 $^\circ\text{C}$ with defined heating rates. Turbidity was measured in a quartz cuvette (10-mm path length). Three parameters were extracted from the curves: the maximum turbidity at steady state, the rate of assembly, and the lag time between the temperature jump and the start of the turbidity rise. Three experiments were performed and averaged.

Fourier Transform Infrared Spectroscopy—The preparation of samples for FTIR was performed as described (25). FTIR experiments were performed on a Jasco FT-IR410 instrument (Jasco, Gross-Umstadt, Germany). Atmospheric water vapor was removed by flushing the spectrometer with nitrogen. Interferograms were mostly recorded between 1700 and 1600 cm^{-1} at a spectral resolution of 1 cm^{-1} , and 128 spectra were averaged. They were acquired in the transition mode using CaF_2 cells, separated by spacers of different thicknesses (usually 25 μm). After recording a reference spectrum of the instrument and of the D_2O lot used, the protein solutions were applied, and

the absorbance spectrum of the sample was measured. The water vapor background was subtracted from the D_2O spectra and the sample spectra before subtracting the D_2O spectra from the sample spectrum. To facilitate comparison the spectra were then normalized with respect to their maxima.

Fluorescence Spectroscopy—All fluorescence experiments were performed on a Spex Fluoromax spectrophotometer (Polytec, Waldbronn, Germany), using 3 \times 3-mm quartz microcuvettes from Hellma (Mühlheim, Germany) with 20 μl of sample volume. For tyrosine excitation spectra, scans ranged from 250 to 300 nm at a fixed emission wavelength of 310 nm, and for emission spectra, scans ranged from 290 to 450 nm at fixed excitation wavelength of 275 nm. For tryptophan excitation spectra, scans ranged from 210 to 310 nm at a fixed emission wavelength of 350 nm, and for emission spectra, scans ranged from 300 to 400 nm at fixed excitation wavelength of 290 nm. In all cases, the slit widths were 5 nm and integration time was 0.25 s, and photomultiplier voltage was 950 V. Preparations of samples for fluorescence spectroscopy were similar to those used for FTIR.

Fluorescence Quenching Experiments—Steady-state fluorescence quenching experiments were performed on either soluble or aggregated proteins. Aliquots of the stock quenching solutions (5 M) were added into the cuvette containing 10 μM protein in PBS, pH 7.4. Quenching experiments were performed with excitation at 280 nm. Stock quenching solutions were freshly prepared at concentrations of 5 M. Quenching data were fitted to the Stern-Volmer equation, $F_0/F_c = 1 + K_{SV}[Q]$, where F_0 and F_c are the fluorescence intensity in the absence and in the presence of quencher, $[Q]$, at concentration c , respectively, and K_{SV} is the Stern-Volmer quenching constant.

Denaturation and Disassembly of PHFs by GdnHCl—For the disaggregation of PHFs, preformed PHFs were centrifuged at 100,000 $\times g$ for 30 min at room temperature (table top centrifuge TL-100, Beckman) and resuspended in PBS. 10 μM of this PHF solution was diluted with GdnHCl (stock solution of 8 M) to various concentrations, incubated at 37 $^\circ\text{C}$ overnight, and analyzed the next day. To circumvent inconsistencies due to variations in concentrations, the emission spectra were normalized to their maximum.

RESULTS

Trp Residues in the Repeat Domain of Tau Are Sensitive Reporters of the Stages of PHF Aggregation—The structure of tau is currently not known because it is not amenable for x-ray crystallographic or NMR analysis. Our earlier results, based on x-ray solution scattering, CD, and FTIR spectroscopy, have suggested that soluble tau has a mostly random coil structure and that aggregation into PHFs is accompanied by a shift in conformation to a substantial β -sheet content (25–27). The sequences involved in the conformational transition are located within the repeat domain of tau (hexapeptide motifs PHF6* (Val²⁷⁵–Lys²⁸⁰) in the second repeat and PHF6 (Val³⁰⁶–Lys³¹¹) in the third repeat). In principle such changes could be monitored by fluorescence changes, notably that of tryptophan because of its sensitivity to the local environment. Unfortunately, tau contains very few aromatic amino acids. The longest isoform htau40 consists of three phenylalanines (Phe⁸, Phe³⁴⁶, and Phe³⁷⁹), five tyrosines (Tyr¹⁸, Tyr²⁹, Tyr¹⁹⁷, Tyr³¹⁰, and Tyr³⁹⁴), and no tryptophan. None of these lie in alternatively spliced regions so that all tau isoforms have the same aromatic residues. In order to measure the impact of PHF formation on the fluorescence, we introduced tryptophans into different sites within the repeat domain (Fig. 1C) because this is crucial for PHF assembly (6, 9, 13, 16, 28, 29). In most cases we performed conservative exchanges at aliphatic (L266W, I297W, and I328W) or aromatic amino acids (Y310W and F346W), except for Q244W, with the aim of minimizing any perturbation in the protein structure (Fig. 1C). Because of the prominent role of the hexapeptide motifs PHF6 and PHF6* in PHF assembly, we were especially interested in the impact of PHF formation on tryptophan in these sequences.

The fluorescence spectra of the repeat domain construct K18 (containing the single tyrosine Tyr³¹⁰ within the PHF6 hexapeptide motif but no tryptophan) and the spectra of mutated K18-Y310W are shown in Fig. 2. The tyrosine containing

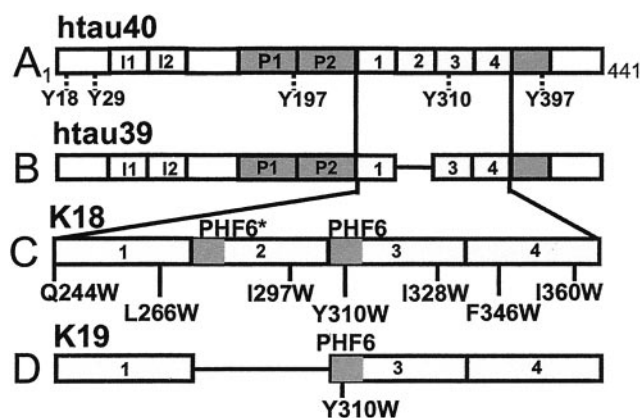


FIG. 1. Bar diagram of tau isoforms, tau constructs and tryptophan mutants. *A*, full-length isoform httau40 (largest isoform in human central nervous system, containing two alternatively spliced inserts near the N terminus (*I1* and *I2*) and 4 repeats (*R1*–*R4*) in the C-terminal half; 441 residues) (54). The protein contains 5 Tyr residues (18, 29, 197, 310, 397, indicated above bar), but no Trp. Tyr³¹⁰ is the only one in the repeat domain. The mutant Y310W generates intrinsic Trp fluorescence without inhibiting aggregation (see below). *B*, isoform httau39 (only three repeats due to alternative splicing of exon 10 so that *R2* is removed). It contains the same 5 Tyr residues as httau40. *C*, enlarged view of repeat domain (construct K18, four repeats only, 129 residues, Gln²⁴⁴–Glu³⁷²). *D*, repeat domain construct K19, three repeats only, 94 residues, Gln²⁴⁴–Lys²⁷⁴ and Val³⁰⁶–Glu³⁷². The numbering is according to httau40, the longest isoform in human central nervous system containing 441 residues. The dark gray areas flanking the repeats shown for httau40 and httau39 represent the basic and proline-rich domains that contribute strongly to microtubule binding (“jaws” (23)). The dark gray boxes in K18 and K19 show the hexapeptide motifs PHF6* (275VQIINK²⁸⁰) and PHF6 (306VQIVYK³¹¹) whose conversion to β -structure is an early step in PHF assembly (25, 27). The mutation Y310W (in repeat *R3*) was introduced in all isoforms. Mutations Q244W, L266W, I297W, I328W, F346W, and I360W covering positions along the whole sequence of the repeat domain are indicated for K18.

K18 exhibits only a small change in the fluorescence spectrum during PHF assembly, showing a slight red shift of ~2–3 nm (Fig. 2, *A* and *B*). Although this effect is detectable, it is too small to serve as a reliable marker of PHF assembly. By contrast, the mutant K18-Y310W shows a clear shift upon PHF assembly, equivalent to a blue shift of ~15 nm from 354 nm in the soluble state to 339 nm in the polymerized state. The positions of the excitation and emission maxima, 288 and 354 nm, indicate that the Trp residue is almost fully exposed to the solvent in the soluble state and not buried in the interior of the protein. The blue shift following PHF aggregation is explained by an increased hydrophobicity in the local environment (30, 31); it suggests that Trp³¹⁰ becomes buried in a hydrophobic pocket within the PHFs.

Similar results to the repeat domain K18 were obtained with the full-length isoforms httau40 and httau39 (lacking *R2*). The unmodified proteins contain five Tyr residues (Tyr¹⁸, Tyr²⁹, Tyr¹⁹⁷, Tyr³¹⁰, and Tyr³⁹⁴) whose fluorescence spectra are essentially the same as in K18 (data not shown, see Fig. 2, *A* and *B*). However, when a Trp is introduced at residue 310 it dominates the spectrum. In the soluble state, the excitation and emission maxima are 288 and 352 nm, indicating almost full solvent exposure. This means that Trp³¹⁰ does not become embedded in other domains of the protein, even in the full-length protein. When httau40 is aggregated into PHFs, a blue shift down to 334 nm is observed (Fig. 2*E*). This shift is even more extensive than that of K18 and suggests effective burial of the tryptophan in a hydrophobic pocket inside the PHFs.

A similar, although less extensive, blue shift is observed with the Y310W mutant of httau39 (from 352 nm in the soluble to 342 nm in the polymerized state, Fig. 2*F*). In summary, these results are consistent with an open structure of the repeat

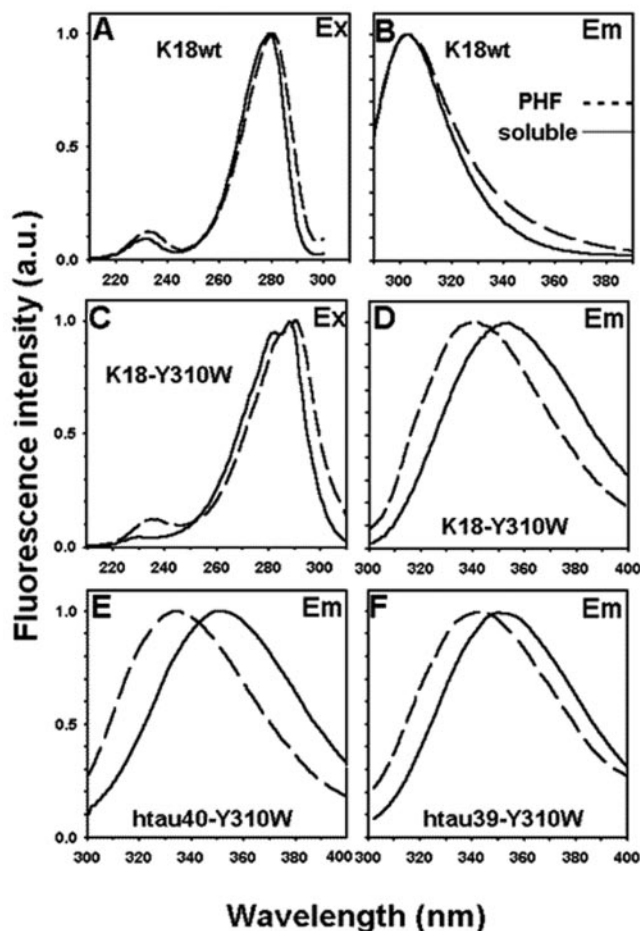


FIG. 2. Tyrosine and tryptophan fluorescence spectra of the 4-repeat constructs K18wt and K18-Y310W and of the full-length isoforms httau39-Y310W and httau40-Y310W before and after PHF assembly. *A* and *B* show the excitation (*Ex*) and emission (*Em*) spectra of construct K18wt in the soluble state (*solid curve*) and after PHF assembly (*dashed*), normalized to the same height (peaks at ~280 and ~305 nm, respectively). The fluorescence is entirely due to the single Tyr³¹⁰ that shows a slight red shift upon aggregation. *C* and *D* show the equivalent excitation and emission spectra for the mutant K18-Y310W. *C* shows an excitation scan with emission fixed at 350 nm, which peaks at 290 nm. *D* shows the emission scan with excitation at 280 nm. The spectra exhibit a maximum at 354 nm for the soluble and 339 nm for the aggregated protein. Note the significant blue shift of the emission maximum in *D* following PHF assembly (~15 nm, from 354 to 339 nm). *E* and *F* show the emission spectra of the isoform mutants httau40-Y310W and httau39-Y310W (excitation at 290 nm). Even in the full-length isoforms the spectra are dominated by the single tryptophan and show the pronounced blue shift upon PHF assembly (*dashed curves*).

domain in the soluble state and with its burial inside the PHFs during aggregation. All the other tryptophan single mutations show blue shifts from the soluble to the aggregated state whose magnitude depends on the site of mutation (see Fig. 7).

Trp Mutants Display Similar Kinetics of Aggregation, Conformational Transitions, and Microtubule Interactions as Wild-type Tau—Introducing mutants into the structural analysis of tau and PHFs requires evidence that the mutation does not alter the specific activities of the protein. We will illustrate this by data on PHF assembly, PHF morphology, analysis of the conformation of soluble and polymerized protein, and effects on MT assembly. In our earlier studies on PHF aggregation, we made use of the accelerating effect of polyanions and monitored aggregation by the fluorescence of the added dye thioflavine S (17). Thus, for the present study we checked whether the Trp mutants would behave similarly by the same criteria. Fig. 3

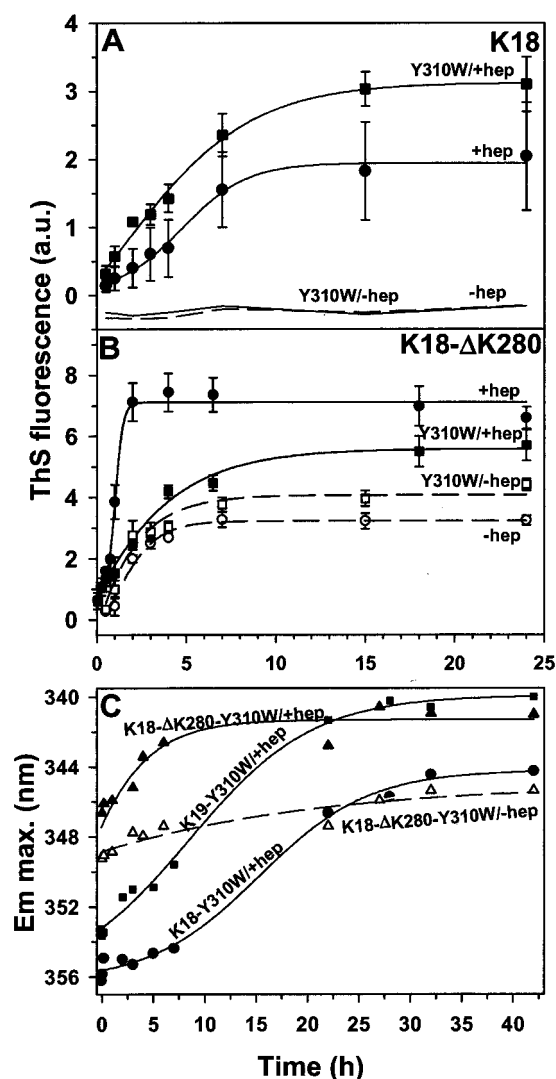


FIG. 3. Time course of PHF assembly from constructs K18 and K19 followed by ThS and tryptophan fluorescence. *A*, kinetics of PHF formation of K18 in the presence of heparin (*hep*) (filled circles, middle curve) or without heparin (*dashed curve*, bottom); and kinetics of K18-Y310W in the presence of heparin (filled squares, top curve) or without heparin (solid line, bottom) measured by ThS. Note that both the wild-type and the Trp mutant require polyanions (heparin) for efficient polymerization and that the time course of assembly is similar, even though the extent differs. *B*, kinetics of PHF assembly of construct K18- Δ K280 with or without heparin (filled circles, top curve, and empty circles, bottom curve); and kinetics of K18- Δ K280-Y310W with or without heparin (filled and empty squares, middle curves). The Δ K280 mutation allows both proteins to polymerize even without heparin, but heparin accelerates the process. *C*, kinetics of PHF formation observed by tryptophan fluorescence in Y310W mutants of K18 and K19 (excitation at 290 nm, emission scan 300–420 nm, wavelength of emission maximum is plotted versus time). The proteins containing the Δ K280 mutations (K18- Δ K280-Y310W, filled and open triangles) aggregate rapidly and start from a lower maximum wavelength (\sim 348 nm) than K18-Y310W and K19-Y310W (start at 355 and 353 nm, respectively).

illustrates that this is the case for PHF assembly, with only minor modifications. The repeat domain K18 aggregates with roughly similar kinetics, with or without the Y310W mutation; in both cases added polyanions (heparin) are needed to achieve efficient aggregation (Fig. 3A). The result is noteworthy because residue 310 is part of the hexapeptide motif VQIVYK involved in the generation of β -structure during aggregation. Apparently the exchange of Tyr to Trp does not destroy the capacity of the motif to support aggregation, in contrast to Pro mutations (27). Next we checked the K18- Δ K280 mutant. This

mutant was discovered in a search for FTDP-17 mutations (32); it is particularly interesting for *in vitro* studies because this mutation is highly efficient for PHF assembly (24) even without polyanions (25). Here, too, we find that the Y310W mutation has little influence on the behavior of the protein. In either case it is able to aggregate into PHFs with similar kinetics without polyanions, although added heparin still has an accelerating effect (Fig. 3B).

By having shown that the Y310W mutation leaves the capacity for PHF formation intact, we tested whether the fluorescence of Trp³¹⁰ could serve as an intrinsic reporter of aggregation. Fig. 3C shows the wavelength of the emission maximum during the time course of aggregation. Soluble K18 and K19 begin at values of \sim 354–356 nm and change gradually toward final values of \sim 340–346 nm (filled circles and squares). The half-times, \sim 10 h, are of comparable magnitude but longer than the values obtained with ThS fluorescence (\sim 5 h, see Fig. 3A), indicating that these two fluorophores emphasize somewhat different aspects in the aggregation process.

A likely interpretation is that the fluorescence of Trp³¹⁰ or ThS responds differently to intermediate steps in PHF formation (e.g. dimerization, nucleation, and annealing). In addition, the weighting of the assembly states is different. In the case of Trp³¹⁰, all molecules contribute, resulting in an overlap of spectra with different emission maxima. In the case of ThS, the spectrum is dominated by molecules attached to aggregates, whereas the contribution of monomers, dimers, and low oligomers is thought to be negligible. Thus, it is possible that incipient aggregation is highlighted by ThS but not by the intrinsic fluorescence of Trp. The mixture of aggregation states is well illustrated by the curves of the K18- Δ K280 mutants (Fig. 3C, open and filled triangles) which start already midway on the y axis, around 348 nm. This is due to the high tendency of this mutant to aggregate, so that oligomers and small aggregates become noticeable even at the earliest time points. Note that K19-Y310W reaches the same extent of polymerization as K18- Δ K280-Y310W in the presence of heparin regarding the emission maximum, whereas K18-Y310W in the presence of heparin behaves similar to K18- Δ K280-Y310W in the absence of heparin. This shows one advantage of the Trp fluorescence in comparison to the ThS fluorescence because the extent of the shift is defined as the ratio of the soluble to the aggregated protein (the exact values for the aggregated protein are taken from Table I, for which PHFs were pelleted and measured without contamination of soluble protein). The extent of polymerization for the proteins was calculated from the relative shift in the emission maximum (Fig. 3C): K19-Y310W 93%, K18-Y310W 54%, K18- Δ K280-Y310W 56% in the absence of heparin, and 89% in the presence of heparin. Note that with the Trp fluorescence no centrifugation step was needed to determine the efficiency of polymerization.

Because proteins can often aggregate in different forms we ascertained that, in the conditions chosen here, the aggregation products were indeed PHFs or related structures. Fig. 4 shows a panel of fibers assembled from different K18 mutants. They show the morphology and variability of PHFs assembled *in vitro*, i.e. widths between 10 and 20 nm, a twist which can be variable (between 50 and 200 nm), or even “straight fibers” similar to those that are also observed in Alzheimer’s disease. In addition there are frequent short fiber stubs (100–200 nm) that may be breakdown products during specimen preparation. All of these features are typical of PHFs obtained from Alzheimer brain or reassembled from wild-type tau, indicating that the Trp mutations do not alter the building plan of the assembly reaction.

The aggregation of tau into PHFs is accompanied by the

TABLE I
Parameters of intrinsic Trp fluorescence of different tau derivatives

Mutants	Emission maximum in soluble state (Ex at 290 nm)	Emission maximum in PHF state (Ex at 290 nm)	Midpoint of denaturation GdnHCl	Slope (<i>K</i>) of quenching by acrylamide, soluble state	Slope (<i>K</i>) of quenching by acrylamide, PHF state
			<i>M</i>		
K19-Y310W	353	340	1.2	N.D.	N.D.
K18-Y310W	355	339	1.1	13.8	4.2
K18-ΔK280-Y310W	348	339	1.8	9.0	3.7
K18-Q244W	354	342	1.5	11.3	7.1
K18-L266W	353	341	1.3	13.6	8.0
K18-I297W	352	332	1.8	13.5	3.6
K18-I328W	352	340	1.6	11.0	5.0
K18-F346W	352	349	1.0	13.6	9.2
K18-I360W	354	352	1.0	12.0	11.2
ht40-Y310W	352	334	1.0	13.0	3.7
ht39-Y310W	350	342	0.5	16.5	8.1

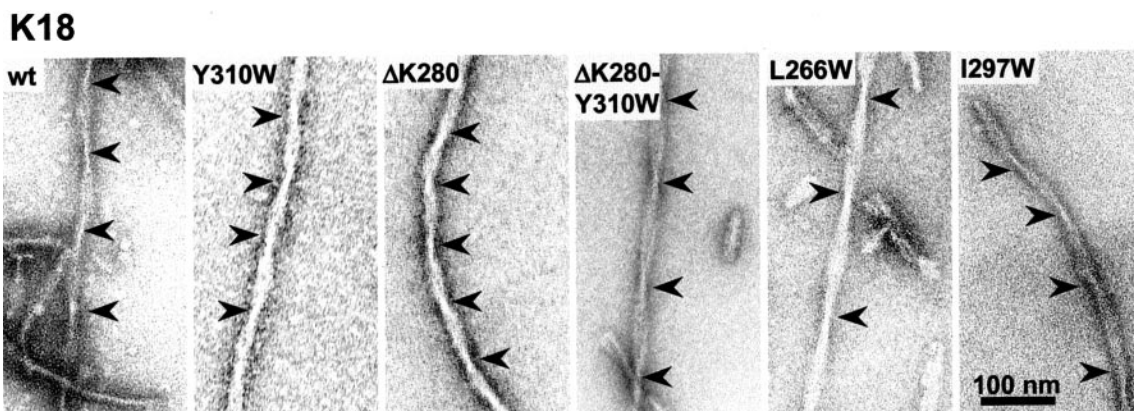


FIG. 4. Filaments polymerized from the repeat domain and mutants containing tryptophan have typical paired helical appearance. Panels from left to right show negative stain electron micrographs of K18wt, K18-Y310W, K18-ΔK280, K18-ΔK280-Y310W, K18-L266W, and K18-I297W. The images show that all K18 mutants aggregate into similar PHF structures. There is some variation in the degree of twisting, but this is not correlated with the type of mutant. *wt*, wild type.

formation of local β -structure around the hexapeptide motifs ²⁷⁵VQIINK²⁸⁰ and ³⁰⁶VQIVYK³¹¹. Mutations in these regions can have a strong influence on PHF aggregation, either favorable (e.g. ΔK280, P301L, both found in frontotemporal dementias) or unfavorable (any proline mutation (24, 27)). It was therefore important to ascertain whether the Y310W mutation or any of the other Trp mutations (Fig. 1) had an influence on β -structure formation. This was investigated by FTIR spectroscopy. The spectrum of the soluble wild-type K18 protein exhibits a maximum at ~ 1652 wavenumbers (*solid line* in Fig. 5A) indicating mostly random coil structure (33). During aggregation it is shifted to lower values, ~ 1630 cm^{-1} (*dashed line* in Fig. 5A), a typical behavior for increasing β -structure (34). The tryptophan mutant K18-Y310W shows a comparable shift (although not as prominent, with only a shoulder at 1625 cm^{-1} , *dashed line* in Fig. 5B), and indeed all of the Trp mutants of K18 gave similar results (examples of K18-I297W and K18-I360W are shown in Fig. 5, C and D). It is therefore likely that all mutants pass through similar intermediate stages during their aggregation into PHFs. Note that the change in conformation is nearly invisible for full-length tau because the fraction of β -structure is too low (27).

One of the physiological roles of tau is to stabilize neuronal microtubules. This function involves the repeat domain (8, 23, 35) and can be observed *in vitro* by UV light scattering from assembling microtubule solutions. We asked whether the Trp mutations in the repeat domain would impair the assembly-promoting function of tau. Fig. 6 illustrates for the case of the Y310W that the results with or without the mutation are nearly indistinguishable. Tubulin alone does not self-assemble in these conditions (*filled circles*), but assembly is strongly

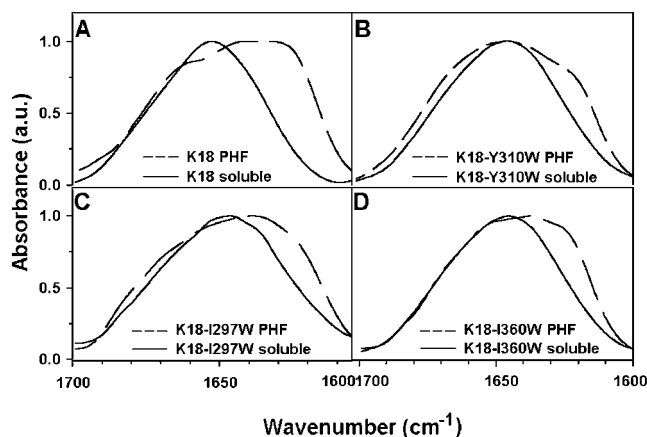


FIG. 5. FTIR spectra of PHF and soluble tau protein of Trp mutants. A–D, K18wt, K18-Y310W, K18-I297W, K18-I360W. The soluble proteins (*solid lines*) have maxima around 1652 cm^{-1} ; polymerization (*dashed lines*) shifts the curves to the right (lower wavenumbers), indicating an increase in β -structure.

enhanced by htau40 or its Y310W mutant (half-time ~ 0.5 min, *open triangles* and *squares*). A similar result applies to htau39, except that the assembly stimulation is less pronounced, consistent with the absence of one repeat, R2 (half-time ~ 1.2 min, *filled triangles* and *squares*). Note that these experiments cannot be carried out with the repeat domain alone (K18 or its mutants) because its binding to microtubules and its capacity of inducing microtubules is too weak at the concentrations used here when the other flanking domains of tau are absent (23). In

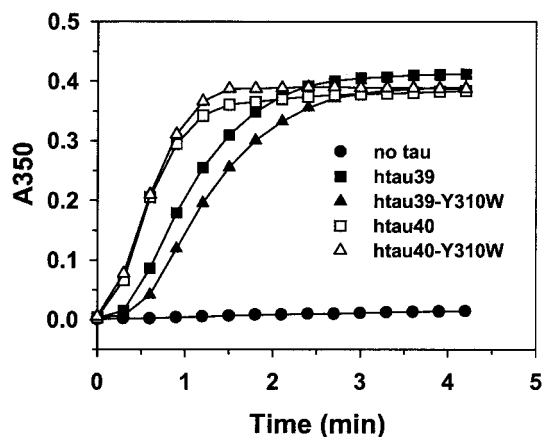


FIG. 6. Microtubule assembly induced by tau or Y310W mutants. Assembly of microtubules from tubulin was induced by a temperature shift to 37 °C and measured by light scattering (absorption at 350 nm). Without tau, tubulin does not self-assemble at the chosen concentration (30 μ M tubulin heterodimer, filled circles, bottom curve). Both tau isoforms htau40 and htau39 (5 μ M) are competent to induce microtubule assembly (open and filled squares), and the Y310W mutation does not affect the efficiency in either case (htau40-Y310W, open triangles, and htau39-Y310W, filled triangles).

summary, the Trp mutations introduced into the repeats of tau have little effect on the structure and functions of tau that matter for PHF aggregation or microtubule assembly. Therefore, these mutations can be regarded as valid reporters on conformations and assembly states of tau.

Trp Mutants Spanning the Repeat Domain Highlight the Importance of the Second and the Third Repeat for the PHF Core—Because the repeat domain forms the core of PHFs, one may expect that its residues become buried within the PHF structure. The degree of solvent exposure before and after aggregation can be monitored by means of a fluorescence quenching agent, *e.g.* acrylamide. We generated 7 Trp mutants of K18 distributed over the molecule, and we measured their accessibility to the quencher. In this type of experiment a Stern-Volmer plot displays the ratio of F_0 to F_c (without/with quencher at concentration c) as a function of the quencher concentration. Fig. 7A shows Stern-Volmer plots of the aggregated proteins, and Fig. 7B shows the slopes *versus* the sequence position of the Trp mutants. All the soluble proteins exhibit nearly the same slopes, ~ 11 – 14 (dashed line), indicating almost maximal accessibility (free tryptophan exhibits a slope of 17, not shown). By contrast, the slopes of the polymerized proteins are much lower, they vary from 3 to 10 (solid lines). The plot of slopes *versus* sequence position appears roughly U-shaped, with minimal values in repeats R2 and R3 (mutations I297W, Y310W, and I328W, slopes 4–5) and higher values toward the two ends, R1 and R4 (Q244W, L266W, F346W, and I360W). More specifically, the two mutants with the tryptophan within the first repeat show a lower slope than those in the fourth repeat, and the slope for the I360W mutant near the C-terminal end of the repeats is almost maximal, indicating full solvent accessibility even after PHF assembly. Thus the quenching experiments emphasize the importance of the second and third repeat for building the PHF core.

The above conclusions are confirmed independently by analyzing the wavelength shift of the different Trp mutants before and after PHF aggregation (Fig. 7C). The soluble proteins (filled circles) exhibit emission maxima of ~ 352 nm with very little variation. By contrast the emission maxima of the polymerized proteins show a strong dependence on sequence, with the largest blue shift (to 332 nm) for the mutant I297W and the smallest shift (to 350 nm) for I360W. Remarkably, the curve of

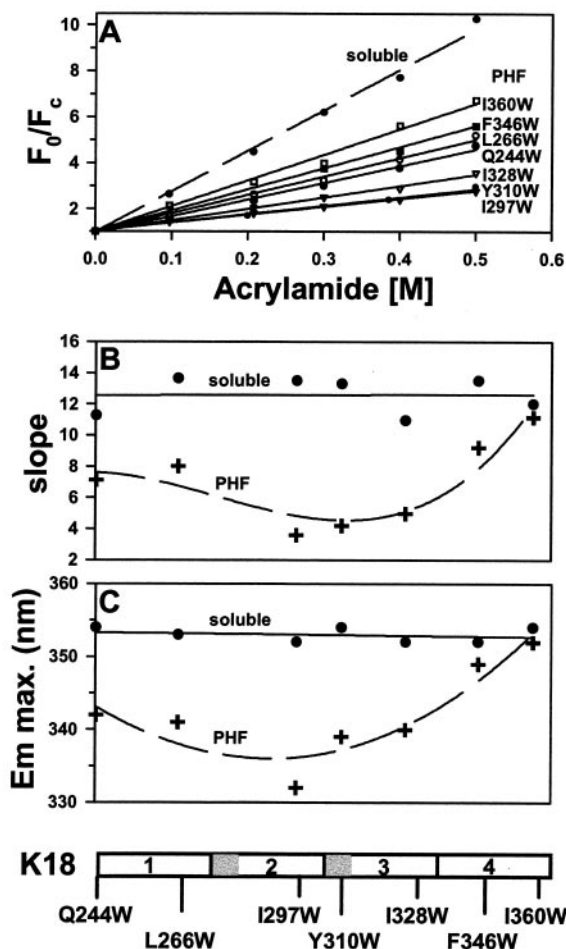


FIG. 7. Solvent accessibility of tryptophans in the repeat domain of tau in the soluble state and after PHF aggregation. Seven residues, distributed over the repeat domain (construct K18), were mutated into tryptophans and probed for their exposure to the solvent (Gln²⁴⁴, Leu²⁶⁶, Ile²⁹⁷, Tyr³¹⁰, Ile³²⁸, Phe³⁴⁶, and Ile³⁶⁰) before and after aggregation. Excitation 290 nm, emission scan 300–420 nm, with maxima around 350 nm. A, fluorescence quenching by acrylamide of PHFs formed from K18 mutants, represented as Stern-Volmer plot $F_0/F_c = 1 + Kc$ (c = acrylamide concentration). A high slope K indicates high solvent accessibility. The top curve (dashed line) shows one example of soluble protein (K18-I360W), exhibiting the maximum slope of 13. The solid curves represent seven mutants of K18 in the polymerized states, with significantly lower slopes depending on the position of the Trp residue (slopes between 4 and 10, see B), indicating reduced solvent exposure. B, dependence of solvent accessibility (slopes in A) on position of Trp residue along sequence. The slopes of the soluble proteins show no systematic dependence on the sequence (filled circles, solid line on top), showing that no shielded pockets are detectable. After PHF assembly (+ symbols, dashed line), a U-shaped curve emerges, illustrating that the residues near the ends of the sequence (in R1 and R4) are more exposed than those in the middle (in R2 and R3). Most of the residues are more buried in the PHF state than in the unpolymerized state (except I360W). C, dependence of emission maximum wavelength on position of Trp residue along sequence. For the soluble proteins (filled circles, solid line on top) the maxima are around 350–355 nm, indicating full solvent accessibility. After PHF assembly (+ symbols, dashed line), the emission maximum shows a pronounced blue shift. As in B there is a U-shaped dependence on the position of Trp in the sequence, arguing that the residues in the middle are more shielded than those at the edges of the repeat domain.

wavelength shift *versus* sequence has almost the same U-shape as the quenching slopes (Fig. 7B). This demonstrates that the emission maximum is a reliable sensor of the local environment, and that repeats R2 and R3 (notably residue 297) become buried in the PHF structure, whereas the tail (residues 346, 360) is nearly exposed to the solvent.

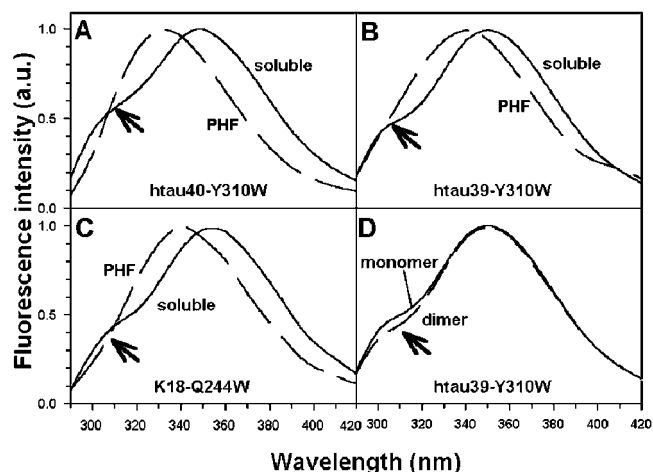


FIG. 8. Interactions of hexapeptide motifs analyzed by FRET between Tyr and Trp. K18 mutation series and httau39-Y310W and httau40-Y310W were used to analyze FRET between Tyr and Trp in soluble and polymerized tau protein. Tau proteins containing the Y310W mutation were irradiated at 275 nm which excites both the Tyr and Trp fluorescence. **A**, in the soluble state of httau40-Y310W (*solid curve*), the combined fluorescence of Tyr¹⁸, Tyr²⁹, Tyr¹⁹⁷, and Tyr³⁹⁷ is visible as a shoulder at ~305 nm on the dominant fluorescence of Trp³¹⁰ peaking at 350 nm. Upon PHF aggregation (*dashed curve*), the Trp³¹⁰ spectrum shows the characteristic blue shift due to the burial of the residue, and the shoulder at 305 nm disappears because the tyrosines are now within the Förster distance and transfer their energy to the tryptophan. **B**, fluorescence spectra of httau39-Y310W in the soluble (*solid line*) and PHF state (*dashed line*), showing similar behavior as httau40-Y310W. **C**, construct K18-Q244W exhibits FRET from the single Tyr³¹⁰ to Trp²⁴⁴ upon PHF assembly, similar to full-length tau isoforms above (soluble protein, *solid line*, and polymerized protein, *dashed line*). **D**, the emission spectra of the monomeric and the dimeric mutant of httau39-Y310W (separated by gel filtration) are shown (monomer, *solid curve*, and dimer, *dashed curve*). Note that there is no significant difference, indicating that dimerization alone does not bring Tyr residues into proximity of Trp.

FRET Shows That during Tau Aggregation the N- and C-terminal Regions Approach the PHF Core—The analysis of antibodies raised against Alzheimer tau has suggested a “pathological” conformation where regions outside the repeat domain can fold over the repeat domain, *e.g.* Alz50, MC-1, and SMI-34 (36–39). Because we placed a tryptophan within the repeat sequence (Y310W), it is now possible to look at the interaction of different domains by FRET analysis using the resonant energy transfer from tyrosines to tryptophan. Full-length tau contains 5 tyrosines (Tyr¹⁸, Tyr²⁹, Tyr¹⁹⁷, Tyr³¹⁰, and Tyr³⁹⁴); after replacement of Tyr³¹⁰ 4 Tyr residues remain, most of them are located in the N-terminal half. The results in Fig. 8 show that there is a difference between soluble and aggregated httau40-Y310W (Fig. 8A, *solid* and *dashed lines*). The soluble protein shows a maximum at 352 nm, as expected from the fluorescence of Trp³¹⁰, and an additional shoulder around 305 nm representing the fluorescence of the combined tyrosines. In principle, Trp could take up the fluorescence from nearby Tyr residues closer than the Förster distance (1 nm for Tyr/Trp as the donor/acceptor pair (40, 41)). Conversely, the existence of a pronounced shoulder implies that most Tyr residues are sufficiently far from Trp³¹⁰ to prevent the FRET effect. A different result is obtained for the polymerized protein. The emission maximum shows the blue shift described above, but in addition the tyrosine shoulder disappears (*dashed line*). This implies that the Tyr residues are now close enough to Trp³¹⁰ to allow energy transfer by FRET. At present it is not possible to distinguish whether the transfer occurs within a molecule or between neighboring molecules (this will be investigated by generating more donor/acceptor pairs), but the result

emphasizes the close approach of the outer regions of tau (N- and C-terminal tails) to the PHF core formed by the repeat domain. A similar behavior is found for httau39-Y310W (Fig. 8B), *i.e.* no or little FRET in the soluble state and therefore a shoulder at 305 nm which becomes deleted by FRET in the aggregated state.

A different situation applies to the Trp mutants of K18 (Fig. 8C). In this case there is only one Tyr, Tyr³¹⁰, that acts as the donor, and Trp introduced at other positions can serve as acceptor (at residues 244, 266, 297, 328, 346, or 360, Fig. 1C). In all cases, the shoulder at 305 nm (*arrows*) is weak or absent because the single Tyr is dominated by the Trp fluorescence. A weak shoulder can be discerned with the Q244W mutant in the soluble state that disappears after aggregation (Fig. 8C). This argues that residue 244 at the beginning of the repeats is far from residue Tyr³¹⁰ within any given molecule (because FRET is absent in the soluble state) and approaches Tyr³¹⁰, probably of neighboring molecules, during PHF aggregation. By contrast, Trp³¹⁰ shows a 305 nm shoulder both in the soluble and aggregated state (data not shown), indicating that the C-terminal end of the repeats remains far from Tyr³¹⁰ in both states. Finally, in the cases of the more centrally located Trp residues (266, 297, 328, and 346) FRET occurs both in the soluble and aggregated state (data not shown), likely because these residues are near Tyr³¹⁰ in all conditions. Together, the data argue that (a) residues at the edges of the repeat domain (266, 360) are far from the center (Tyr³¹⁰) in individual molecules, (b) residue 244 approaches the PHF core during aggregation but residue 360 remains far, and (c) the more internal residues are spatially near the center. Because the Förster distance of 1 nm is equivalent to the spacing of 2–3 residues, the results also suggest that the repeat domain must be folded rather than being extended.

PHF assembly is greatly enhanced by tau dimers that can act as building blocks (9, 13). We therefore asked whether spatial relationships can be detected by FRET that distinguish monomers and dimers. A homogeneous solution of dimers can be obtained by oxidation from 3-repeat tau isoforms because they contain only the single cysteine 322. Fig. 8D shows the emission spectrum for tryptophan of monomeric (*solid line*) and dimeric (*dashed line*) httau39-Y310W. Both spectra show a clear shoulder for tyrosine fluorescence at 305 nm, with some reduction in the dimeric state. This means that in the monomeric and dimeric states the tyrosines outside the repeat domain are mostly too far from the tryptophan at position 310 to exhibit FRET. Moreover, there is no blue shift of the maximum, indicating that residue 310 remains in a hydrophilic environment, in contrast to the fully aggregated PHF state (compare *dashed curves* in Fig. 8, A and B).

PHFs from 4-Repeat Isoforms or from FTDP-17 Mutations Show Higher Stability—The pathway of PHF aggregation from soluble tau *in vitro* has been studied by several authors; however, it has been difficult to obtain reliable information on the question of PHF stability. This issue can be addressed using the intrinsic Trp fluorescence. The core of Alzheimer PHFs consists mainly of the repeat domain (7), and one may therefore ask how the composition of the repeats affects PHF stability. We analyzed the thermodynamic stability of PHF assembled from K19 or K18 (3 or 4 repeats) containing the Y310W mutation in the presence of increasing concentrations of guanidine hydrochloride (GdnHCl) (Fig 9). With preformed PHFs the emission maximum is 340 nm in the absence of GdnHCl; at higher GdnHCl concentrations it rises to 354 nm (the value typical of soluble tau) as the PHFs become denatured and disintegrate (this was also checked by SDS-PAGE and electron microscopy, data not shown). K19-Y310W and K18-Y310W

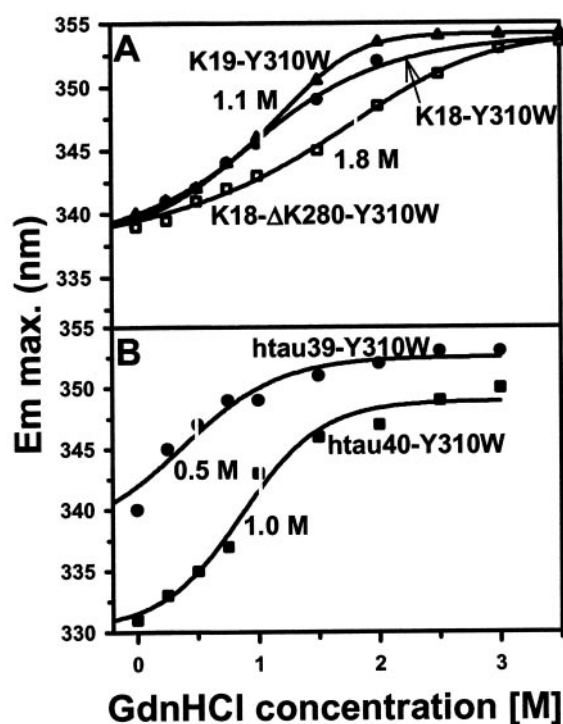


FIG. 9. Stability of PHFs against denaturation by GdnHCl. A, PHFs were first assembled from K19, K18, or K18- Δ K280, each carrying the Y310W mutation as a reporter residue. The emission maximum is plotted *versus* increasing concentrations of GdnHCl. All of them start with emission maxima of \sim 338 nm and were shifted to \sim 353 nm. K19 and K18 show nearly identical stabilities (half-point of denaturation at \sim 1.1 M GdnHCl, *upper curves, filled symbols*), indicating that PHFs made from the repeat domain gain no additional stability from the extra repeat in K18. By contrast, PHFs made from the mutant K18- Δ K280 (carrying one of the FTDP-17 mutations) are much more stable (half-point \sim 1.8 M GdnHCl, *lower curve, open symbols*), consistent with the higher propensity for β -structure. B, disintegration of PHFs made from httau40-Y310W and httau39-Y310W. PHFs made from httau40-Y310W exhibit an initial emission maximum of about 331 nm (*lower curve, squares*), in contrast to httau39-Y310W (*upper curve*) and K19 or K18 (see A). The half-point of denaturation is 0.5 M GdnHCl for httau39-Y310W and 1.0 M GdnHCl for httau40-Y310W. This indicates that the stability of PHFs made from full-length isoforms is higher when four repeats are present (as in httau40) and that PHFs from 3-repeat isoforms (e.g. httau39) are particularly labile.

show half-maximal denaturation at similar GdnHCl concentrations around 1.1 M (Fig. 9A, *filled circles and triangles*). This means that the loss of one repeat in 3R tau does not influence the stability of PHFs made from the repeat domain, even though 3R constructs and isoforms assemble more readily (presumably a kinetic effect, because dimerization and nucleation is faster (17)). By contrast, PHFs made from K18 lacking residue K280 (one of the FTDP-17 mutations) show a significantly higher stability with half-maximal denaturation at 1.8 M GdnHCl (*open squares*). This emphasizes the importance of the β -structure around the hexapeptide motifs which is stabilized by the K18- Δ K280 mutation (25).

To verify these results for full-length tau, we tested the isoforms httau39-Y310W and httau40-Y310W (Fig. 9B). Surprisingly, here the second repeat has a significant impact on stability. PHFs made from httau39-Y310W (3 repeats) started with an emission maximum of 342 nm and red-shifted to 352 nm with a midpoint of 0.5 M GdnHCl. In other words, this construct has only about half the stability of the repeat domain alone. On the other hand, PHFs made from httau40-Y310W shift from an initial 331 nm emission maximum to a final 350 nm with a midpoint of \sim 1.0 M GdnHCl, comparable with that of the repeat constructs alone. Thus there are two interesting differences

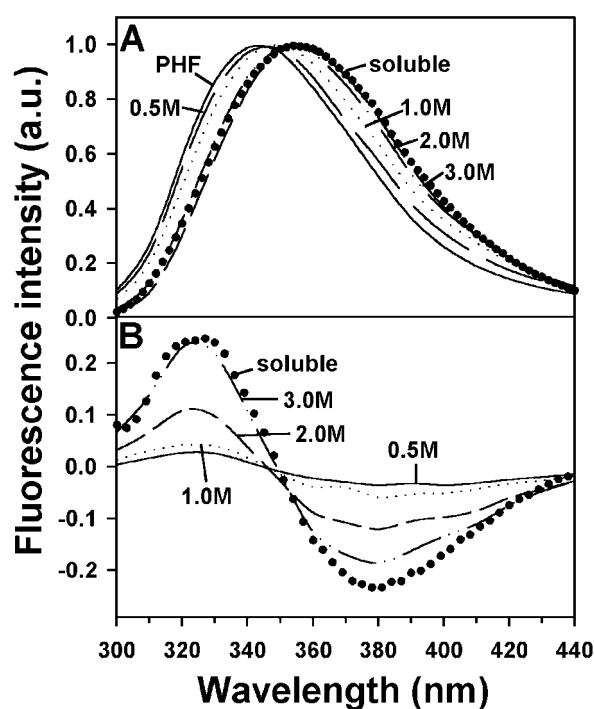


FIG. 10. The intrinsic tryptophan fluorescence can be used to monitor the efficiency of GdnHCl to disaggregate PHFs. PHFs were first formed from K18-Y310W and then exposed to various concentrations of GdnHCl. The disaggregation of PHFs was followed by tryptophan fluorescence as a monitor. The emission spectra are normalized to their maximum. A, emission spectra before PHF assembly (*circles*, emission maximum of 354 nm, excitation at 290 nm), after PHF assembly (*solid line*, emission maximum of 339 nm), and after exposing the PHFs to GdnHCl in different concentrations overnight (0.5 M *medium-dashed line*, 1.0 M *dotted line*, 2.0 M *long-dashed line*, 3.0 M *dash-dot-dot line*). The blue shift from 354 to 339 nm, induced by the initial PHF assembly, is reversed by exposing the PHFs to the GdnHCl. B, difference spectra of the spectra given in A, and all spectra measured in the presence of GdnHCl are subtracted from the spectrum of intact PHFs. The resulting difference curves show a positive maximum around 325 nm and a negative maximum around 380 nm, with an isosbestic point around 350 nm. The example shows that the tryptophan fluorescence can be used to monitor the disassembly of PHFs where other techniques such as ThS fluorescence are not applicable.

between httau39 and httau40 as follows: first, the absolute emission maximum in the PHF state, suggesting a more hydrophobic surrounding in the case of httau40; and second, an increased stability of a 4R isoform *versus* a 3R isoform. It appears as if 3R PHFs are destabilized by factors outside the repeat domain, possibly because the flanking domains cannot be packed tightly enough into the PHF structure.

For potential therapeutic applications it would be interesting to test compounds for their ability to dissolve PHFs. The principle of measuring PHF disaggregation by the intrinsic Trp fluorescence is shown here using the denaturing reagent GdnHCl. More generally this approach can be applied to other inhibitors of PHF formation. As an example, Fig. 10 shows a dose-response curve of PHFs in the presence of various concentrations of GdnHCl. The data points were taken from the curves shown in Fig. 9. The emission maxima in the presence of rising concentrations of GdnHCl become increasingly red-shifted, concomitant with the disintegration of PHFs (Fig. 10A). Fig. 10B shows difference spectra (before and after incubation with GdnHCl) of the normalized spectra of PHFs preassembled from K18-Y310W in the presence of GdnHCl concentrations ranging from 0.5 to 3 M. The difference maxima at 325 (positive) and 380 nm (negative) increase with rising GdnHCl concentrations. The isosbestic point for all spectra is at 350 nm.

This example shows that the tryptophan fluorescence can be used to monitor the disassembly of PHFs where other techniques like ThS fluorescence cannot be applied.

DISCUSSION

Because abnormally aggregated tau represents one of the hallmarks of Alzheimer's disease and other dementias, it is of obvious importance to study the aggregation mechanism, both from the viewpoint of basic science and for developing methods of intervention. Efforts to study tau aggregation have been hampered mainly by the fact that tau is an unusually hydrophilic and soluble protein, and therefore it aggregates very slowly and inefficiently, if at all, in physiological buffer conditions. Over the past decade several findings have helped to overcome this barrier. (i) Certain domains such as the repeat domain aggregate faster than the intact protein (9, 13), presumably because the repeats form the core of Alzheimer PHFs (6, 7). (ii) Dimerization of tau accelerates aggregation, presumably because dimers have a conformation conducive for tau-tau interactions (9, 13). (iii) Cofactors such as polyanions or fatty acid micelles promote aggregation, apparently by compensating numerous positive charges of tau (12, 14, 15, 42). (iv) Mutations of tau found in FTDP-17 dementias favor aggregation (24, 43, 44, 53). The reasons for this may be heterogeneous, depending on the type of mutation, but at least in the cases of $\Delta K280$ and P301L they can be traced back to an enhanced propensity for β -structure, a feature common to many pathological amyloids (20, 45–47). With these developments it is now possible to form tau aggregates rapidly from recombinant protein and analyze the structure, kinetics, and biochemistry of the process.

A second hurdle in the investigations was the dearth of assay methods of tau aggregation. Electron microscopy is slow, difficult to quantify, and limited in resolution and therefore not well suited for kinetic and structural analysis, although it is important for distinguishing fibers with "paired helical" appearance from other types of aggregates. Spectroscopic methods (CD and FTIR) are applicable to solutions but are also of limited value because tau does not exhibit pronounced changes between the soluble and aggregated state, due to its mostly random coil structure (1, 26). Two methods that have come into routine use for kinetic studies, together with faster aggregation conditions, are thioflavine S fluorescence and light scattering (17, 42, 44), although here, too, certain limitations apply, for example a low sensitivity to initial states of aggregation. We have therefore searched for alternative methods that would reveal structural aspects of tau and PHFs, and here we report the results obtained with the use of the intrinsic fluorescence of tryptophan. The advantages of this approach can be summarized as follows.

Trp does not occur in normal tau protein, and therefore it can be used as a direct reporter on the local environment when it is inserted by a point mutation.

Trp reports on the local environment by a change in emission maximum and/or fluorescence intensity.

The spectral change can be used to monitor solvent accessibility and thus protein folding and packing during aggregation as well as protein stability, denaturation, or disassembly.

Because Trp can be inserted anywhere it allows analysis of the protein from many local "points of view."

The transfer of fluorescence energy from Tyr to Trp residues serves as a rough marker of distance and thus changes of folding and packing.

Because Trp is an intrinsic component of the protein, it reports on the entire population of protein molecules, including monomers, oligomers, and aggregates.

Trp allows screening of aggregation modifiers (e.g. inhibitors

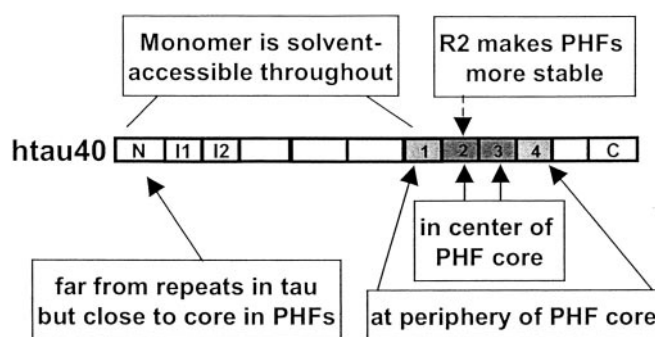


FIG. 11. Summary of structural properties of tau deduced from tryptophan mutants. Judging by fluorescence quenching and emission spectrum, in soluble tau most of the sequence is solvent-accessible; in PHFs the repeat domain becomes buried, especially R2 and R3 which appear to form the center of the PHF core. By FRET and blue shift, residues in R2 and R3 are close to the inner core (marked by Tyr³¹⁰ in the central hexapeptide motif), and those in R1 and R4 are further away but may approach the inner core upon PHF aggregation. Residues near the N- and C-terminal tails of full-length tau are far from the center of the repeat domain but appear to fold back during PHF aggregation. Although the aggregation is triggered by the β -inducing hexapeptide motifs, the stability of PHFs is intrinsically weak, but they can be stabilized by more repeats (i.e. 4R-PHF's are more stable than 3R-PHF's) and FTDP-17 mutations.

or enhancers) independently of other additives (such as thioflavine S whose fluorescence may overlap with that of inhibitor compounds).

In the case of tau the five naturally occurring Tyr residues show only small responses to the state of aggregation and are thus not very useful probes of aggregation (Fig. 2). By contrast Trp inserted into the repeat domain displays a strong signal of aggregation in the form of a blue shift of the emission maximum; the intensity increase ($\sim 10\%$) is relatively small and was not exploited here. The repeat domain is a natural area of Trp insertion because it forms the backbone for PHF aggregation and contains the hexapeptide motifs that play an important role in the local conversion to β -structure when tau aggregates into PHFs. The replacement of Tyr³¹⁰ by Trp is particularly interesting because this lies at the center of the repeat domain and within the PHF6 hexapeptide motif; Trp at position 310 reveals the aggregation process into *bona fide* PHFs without interfering with it (Figs. 3 and 4) and without obstructing the formation of β -structure (as seen by FTIR, Fig. 5). In this regard the insertion of Trp is neutral with regard to aggregation, in contrast to the insertion of prolines into the hexapeptide motifs which prevent aggregation because they are breakers of β -structure (27). As a control, this insertion is also neutral with regard to the ability of tau to promote microtubule assembly (Fig. 6).

Trp inserted into other sites in the repeat domain respond in a qualitatively similar fashion but with notable variations, as shown by the solvent accessibility studies (Fig. 7). Monomeric tau shows almost complete accessibility (judged by the slope of the Stern-Volmer plot). This confirms our previous conclusions from x-ray scattering that tau has a "natively unfolded" structure (26). When Trp residues are inserted in different positions along the repeat domain, all of them become less accessible upon PHF aggregation. This is consistent with the view that the repeat domain becomes packed when tau aggregates into PHFs. Interestingly, the tightest packing occurs in repeats 2 and 3, in the region around residue 300–310 where the hexapeptide motif PHF6 is located, whereas the edges are less tightly packed. In fact residue 360 (end of 4th repeat) remains almost as accessible as the monomeric protein (Fig. 11). This conclusion is reached by two independent criteria (Fig. 7, B and C) and fits well with the concept that the repeat domain

forms the protease-resistant core of PHFs, whereas the regions outside the repeats contribute to the protease-sensitive “fuzzy coat” (6, 7). Refining this concept, the beginning of repeat 1 and the end of repeat 4 are already less tightly packed in PHFs and may represent transition regions to the fuzzy coat, whereas repeats 2 and 3 form the more central part of the PHF core.

One of the challenges in understanding the role of tau is the postulated transition to a “pathological conformation.” Indications for this come from antibodies that recognize early states of Alzheimer degeneration and respond to folded conformations where discontinuous parts of the sequence cooperate to generate the antibody epitope. Examples are antibodies Alz50, MC-1, TG-3, and SMI34 (36–39). We therefore asked if proximities between residues or folded states would be detectable by FRET (Fig. 8). With Trp in position 310 at the center of the repeats, one can ask whether the intrinsic Tyr residues (which are mostly near the N and C termini) are capable of transferring resonance energy to Trp, *i.e.* whether they are located within the Förster distance of ~1 nm for this donor/acceptor pair (40, 41). For monomeric tau the answer is negative, as seen from the independent Tyr fluorescence shoulder around 305 nm. However, upon PHF aggregation the distance becomes smaller than the critical value, and the Tyr shoulder disappears due to the FRET effect. Two interpretations are possible: either tau adopts a more compact folding before aggregation (leading to intramolecular FRET) or the tails of the molecule are constrained to lie near Trp acceptors in neighboring tau molecules in the PHF structure. We tend to favor the second interpretation because of the experiment shown in Fig. 8D; Tau monomers and covalent dimers display a similar Tyr fluorescence shoulder, indicating in both cases a large distance (>1 nm) between the central Trp at position 310 and the Tyr residues in the tails, even though the dimer is already much more assembly-competent than the monomer. Thus, the change from monomer to dimer is not accompanied by a gross change in folding (nor in solvent accessibility), as judged by the Tyr/Trp fluorescence properties. Conversely, the packing is more likely to occur at a later step, *e.g.* PHF nucleation or elongation (16).

Perhaps equally important as the question of PHF aggregation is that of PHF stability and disaggregation because the net load of PHFs in a cell is the result of both opposing processes, and because one may expect a high degree of turnover, at least in the initial stages of the disease (as shown recently for the analogous case of amyloid aggregates (48)). The stability can be probed by exposing pre-formed PHFs to denaturants such as GdnHCl (Fig. 9), with Trp in position 310 as a reporter. One surprising result was that PHF aggregation is readily reversible. A second surprise is that PHF disassembly is achieved by relatively mild denaturation conditions, ~1 M GdnHCl, compared with ~4 M for compact globular proteins such as lysozyme (49). In other words, the initial assembly of PHFs appears rather reversible, and their buildup in cells could probably be prevented if one could avoid stabilization by covalent cross-linking reactions such as glycation (50, 51) or transglutaminase (52). The repeat domain by itself has the same stability with either 3 or 4 repeats, arguing that the extra repeat R2 (exon 10), when present, offers no additional protection for the PHF core *per se* (but see below). As expected, the ΔK280 mutation makes the aggregate almost twice as stable, due to its promotion of β-structure. A somewhat different picture emerges with full-length tau isoforms. PHFs from the 4 repeats isoform httau40 have the same stability as PHFs made from the repeat domain alone, but PHFs from the 3 repeats isoform httau39 are much less stable (0.5 M GdnHCl). This

points to a possible interaction between the tails of tau and the PHF core (note that the N-terminal region of tau, including the inserts of exons 2 and 3, is rather acidic and thus might affect the packing of the basic PHF core). In the context of FTDP-17 dementias the higher stability of 4R-PHF is potentially important because many of these mutations (including the intronic mutations that do not affect protein sequence) lead to an overproduction of 4R-tau isoforms (53) which might therefore increase the level of stable PHFs.

We finally note that Trp reporter constructs might be ideally suited for screening substances capable of inhibiting or reversing PHFs. One reason is that exogenous reporter molecules (like ThS) which might interfere with the test substance are not required. Moreover, test substances are frequently fluorescent by themselves, so that the ThS assay would no longer be applicable. In automated screens this problem could be avoided by intrinsic probes such as Trp.

Acknowledgments—We thank S. Hübschmann for expert technical assistance. We are grateful to Dr. J. Biernat and Dr. S. Barghorn for many helpful suggestions and providing the tau isoforms and constructs used in this study.

REFERENCES

- Cleveland, D. W., Hwo, S. Y., and Kirschner, M. W. (1977) *J. Mol. Biol.* **116**, 227–247
- Mandelkow, E. M., and Mandelkow, E. (1998) *Trends Cell Biol.* **8**, 425–427
- Lee, G., Cowan, N., and Kirschner, M. (1988) *Science* **239**, 285–288
- Goedert, M. (1998) *Prog. Brain Res.* **117**, 287–306
- Kosik, K., Orecchio, L., Binder, L., Trojanowski, J., Lee, V., and Lee, G. (1988) *Neuron* **1**, 817–825
- Wischik, C. M., Novak, M., Edwards, P. C., Klug, A., Tichelaar, W., and Crowther, R. A. (1988) *Proc. Natl. Acad. Sci. U. S. A.* **85**, 4884–4888
- Jakes, R., Novak, M., Davison, M., and Wischik, C. M. (1991) *EMBO J.* **10**, 2725–2729
- Butner, K. A., and Kirschner, M. W. (1991) *J. Cell Biol.* **115**, 717–730
- Wille, H., Drewes, G., Biernat, J., Mandelkow, E. M., and Mandelkow, E. (1992) *J. Cell Biol.* **118**, 573–584
- Wilson, D. M., and Binder, L. I. (1995) *J. Biol. Chem.* **270**, 24306–24314
- DeTure, M. A., Zhang, E. Y., Bubb, M. R., and Purich, D. L. (1996) *J. Biol. Chem.* **271**, 32702–32706
- Perez, M., Valpuesta, J. M., Medina, M., Montejo de Garcini, E., and Avila, J. (1996) *J. Neurochem.* **67**, 1183–1190
- Schweers, O., Mandelkow, E. M., Biernat, J., and Mandelkow, E. (1995) *Proc. Natl. Acad. Sci. U. S. A.* **92**, 8463–8467
- Goedert, M., Jakes, R., Spillantini, M. G., Hasegawa, M., Smith, M. J., and Crowther, R. A. (1996) *Nature* **383**, 550–553
- Kampers, T., Friedhoff, P., Biernat, J., and Mandelkow, E. M. (1996) *FEBS Lett.* **399**, 344–349
- Friedhoff, P., von Bergen, M., Mandelkow, E. M., Davies, P., and Mandelkow, E. (1998) *Proc. Natl. Acad. Sci. U. S. A.* **95**, 15712–15717
- Friedhoff, P., Schneider, A., Mandelkow, E. M., and Mandelkow, E. (1998) *Biochemistry* **37**, 10223–10230
- King, M. E., Ahuja, V., Binder, L. I., and Kuret, J. (1999) *Biochemistry* **38**, 14851–14859
- Garzon-Rodriguez, W., Vega, A., Sepulveda-Becerra, M., Milton, S., Johnson, D. A., Yatsimirsky, A. K., and Glabe, C. G. (2000) *J. Biol. Chem.* **275**, 22645–22649
- Fraser, P. E., McLachlan, D. R., Surewicz, W. K., Mizzen, C. A., Snow, A. D., Nguyen, J. T., and Kirschner, D. A. (1994) *J. Mol. Biol.* **244**, 64–73
- Biernat, J., Mandelkow, E. M., Schröter, C., Lichtenberg-Kraag, B., Steiner, B., Berling, B., Meyer, H. E., Mercken, M., Vandermereen, A., Goedert, M., and Mandelkow, E. (1992) *EMBO J.* **11**, 1593–1597
- Goedert, M., Spillantini, M. G., Jakes, R., Rutherford, D., and Crowther, R. A. (1989) *Neuron* **3**, 519–526
- Gustke, N., Trinczek, B., Biernat, J., Mandelkow, E. M., and Mandelkow, E. (1994) *Biochemistry* **33**, 9511–9522
- Barghorn, S., Zheng-Fischhofer, Q., Ackmann, M., Biernat, J., von Bergen, M., and Mandelkow, E. (2000) *Biochemistry* **39**, 11714–11721
- von Bergen, M., Barghorn, S., Li, L., Marx, A., Biernat, J., Mandelkow, E. M., and Mandelkow, E. (2001) *J. Biol. Chem.* **276**, 48165–48174
- Schweers, O., Schonbrunn-Hanebeck, E., Marx, A., and Mandelkow, E. (1994) *J. Biol. Chem.* **269**, 24290–24297
- von Bergen, M., Friedhoff, P., Biernat, J., Heberle, J., Mandelkow, E. M., and Mandelkow, E. (2000) *Proc. Natl. Acad. Sci. U. S. A.* **97**, 5129–5134
- Ksiezak-Reding, H., and Yen, S. H. (1991) *Neuron* **6**, 717–728
- Rapoport, M., Dawson, H. N., Binder, L. I., Vitek, M. P., and Ferreira, A. (2002) *Proc. Natl. Acad. Sci. U. S. A.* **99**, 6364–6369
- Gasymov, O. K., Abduragimov, A. R., Yusifov, T. N., and Glasgow, B. J. (2001) *Biochemistry* **40**, 14754–14762
- Ropson, I. J., and Dalessio, P. M. (1997) *Biochemistry* **36**, 8594–8601
- Rizzu, P., Van Swieten, J. C., Joosse, M., Hasegawa, M., Stevens, M., Tibben, A., Niermeijer, M. F., Hillebrand, M., Ravid, R., Oostra, B. A., Goedert, M., van Duijn, C. M., and Heutink, P. (1999) *Am. J. Hum. Genet.* **64**, 414–421
- Byler, D. M., and Susi, H. (1986) *Biopolymers* **25**, 469–487
- Susi, H., and Byler, D. M. (1983) *Biochem. Biophys. Res. Commun.* **115**,

- 391–397
35. Goode, B. L., and Feinstein, S. C. (1994) *J. Cell Biol.* **124**, 769–782
36. Carmel, G., Mager, E. M., Binder, L. I., and Kuret, J. (1996) *J. Biol. Chem.* **271**, 32789–32795
37. Jicha, G. A., Bowser, R., Kazam, I. G., and Davies, P. (1997) *J. Neurosci. Res.* **48**, 128–132
38. Lichtenberg-Kraag, B., Mandelkow, E. M., Biernat, J., Steiner, B., Schroter, C., Gustke, N., Meyer, H. E., and Mandelkow, E. (1992) *Proc. Natl. Acad. Sci. U. S. A.* **89**, 5384–5388
39. Abraha, A., Ghoshal, N., Gamblin, T. C., Cryns, V., Berry, R. W., Kuret, J., and Binder, L. I. (2000) *J. Cell Sci.* **113**, 3737–3745
40. Chiu, H. C., and Bersohn, R. (1977) *Biopolymers* **16**, 277–288
41. Eisinger, J. (1969) *Biochemistry* **8**, 3902–3908
42. Wilson, D. M., and Binder, L. I. (1997) *Am. J. Pathol.* **150**, 2181–2195
43. Goedert, M., Jakes, R., and Crowther, R. A. (1999) *FEBS Lett.* **450**, 306–311
44. Gamblin, T. C., King, M. E., Dawson, H., Vitek, M. P., Kuret, J., Berry, R. W., and Binder, L. I. (2000) *Biochemistry* **39**, 6136–6144
45. Lansbury, P. J. (1997) *Neuron* **19**, 1151–1154
46. Pike, C. J., Walencewicz-Wasserman, A. J., Kosmoski, J., Cribbs, D. H., Glabe, C. G., and Cotman, C. W. (1995) *J. Neurochem.* **64**, 253–265
47. Kirschner, D. A., Inouye, H., Duffy, L. K., Sinclair, A., Lind, M., and Selkoe, D. J. (1987) *Proc. Natl. Acad. Sci. U. S. A.* **84**, 6953–6957
48. Hyman, B. T., Smith, C., Buldyrev, I., Whelan, C., Brown, H., Tang, M. X., and Mayeux, R. (2001) *Ann. Neurol.* **49**, 808–810
49. Takano, K., Funahashi, J., and Yutani, K. (2001) *Eur. J. Biochem.* **268**, 155–159
50. Perry, G., Siedlak, S. L., Richey, P., Kawai, M., Cras, P., Kalaria, R. N., Galloway, P. G., Scardina, J. M., Cordell, B., and Greenberg, B. D. (1991) *J. Neurosci.* **11**, 3679–3683
51. Ledesma, M. D., Bonay, P., Colaco, C., and Avila, J. (1994) *J. Biol. Chem.* **269**, 21614–21619
52. Johnson, G. V. W., and Hartigan, J. A. (1998) *Alzheimer's Dis. Rev.* **3**, 125–141
53. Hong, M., Zhukareva, V., Vogelsberg-Ragaglia, V., Wszolek, Z., Reed, L., Miller, B. I., Geschwind, D. H., Bird, T. D., McKeel, D., Goate, A., Morris, J. C., Wilhelmsen, K. C., Schellenberg, G. D., Trojanowski, J. Q., and Lee, V. M. (1998) *Science* **282**, 1914–1917
54. Goedert, M., Spillantini, M. G., Potier, M. C., Ulrich, J., and Crowther, R. A. (1989) *EMBO J.* **8**, 393–399